Numerical Simulation of Richtmyer–Meshkov Instability[*]

I. G. Lebo,[1] V. B. Rozanov,[1] V. F. Tishkin,[2]
V. V. Nikishin,[2] I. V. Popov,[2] and
A. P. Favorsky[2]

[1] The Lebedev Physics Institute (FIAN)
Moscow 117924, Leninsky Pr. 53, Russia

[2] The Institute of Mathematical Modeling
Moscow 125047, Miusskaya sq.4, Russia

Abstract. This paper presents a description of 2D and 3D Euler code "NUT" which is intended for numerical modeling of hydrodynamic instabilities (Rayleigh-Taylor [1, 2] and Richtmyer-Meshkov [3] instabilities). The results obtained for a number of the instability modeling problems are presented. The comparison with the experiment made at G. M. Krzhizhanovsky Power Institute, Moscow is also given.

1   Introduction

The Richtmyer-Meshkov instability (RMI) develops near contact boundaries when a shock wave comes through the disturbed interface between two gases. The numerical modeling of RMI is presented for 2D and 3D contact boundary perturbations.

2   Short Description of the NUT Code

To describe physical processes in the shock tube there has been used a model of non-viscous non-heat-conduction ideal gas which is presented by a system of Euler equations. In vector form, it may be written as follows:

$$\frac{\partial U}{\partial t} + \frac{\partial F(U)}{\partial x} + \frac{\partial G(U)}{\partial y} + \frac{\partial H(U)}{\partial z} = 0 \tag{1}$$

---

where

$$U = \left\{ \begin{array}{c} \rho \\ \rho\mathbf{u} \\ \rho\mathbf{v} \\ \rho\mathbf{w} \\ \rho\left(\varepsilon + \frac{\mathbf{V}^2}{2}\right) \end{array} \right\} \qquad F(U) = \left\{ \begin{array}{c} \rho\mathbf{u} \\ \rho\mathbf{u}^2 + p \\ \rho\mathbf{uv} \\ \rho\mathbf{uw} \\ \rho\mathbf{u}\left(\varepsilon + \frac{\mathbf{V}^2}{2}\right) + p\mathbf{u} \end{array} \right\}$$

$$G(U) = \left\{ \begin{array}{c} \rho\mathbf{v} \\ \rho\mathbf{uv} \\ \rho\mathbf{v}^2 + p \\ \rho\mathbf{vw} \\ \rho\mathbf{v}\left(\varepsilon + \frac{\mathbf{V}^2}{2}\right) + p\mathbf{v} \end{array} \right\} \qquad H(U) = \left\{ \begin{array}{c} \rho\mathbf{w} \\ \rho\mathbf{uw} \\ \rho\mathbf{vw} \\ \rho\mathbf{w}^2 + p \\ \rho\mathbf{w}\left(\varepsilon + \frac{\mathbf{V}^2}{2}\right) + p\mathbf{w} \end{array} \right\}$$

The system is closed by the equation

$$p = (\gamma - 1)\varepsilon\rho. \tag{2}$$

Here, ρ is the density, u, v, w the components of the velocity V; ε the specific internal energy per unit volume, p the pressure, and γ the adiabatic index.

To approximate the system of gas-dynamic equations, we propose using a nonlinear conservative quasi-monotonic explicit difference scheme of a high order of accuracy (analogous schemes for 2D codes have been considered in [4]). The boundary conditions in this scheme are given according to the law: $x = 0, x = L$, then $u = -u$ (reflection condition). The shock wave moves along the Z-axis, $z = Z_{bdry}$, the parameters of the shock wave and shocked gas are calculated from the given Mach number and unshocked gas density and pressure.

The heat conductivity process is described by the following equation:

$$C_v\rho\frac{\partial T}{\partial t} = \frac{\partial}{\partial x}\left(\kappa\frac{\partial T}{\partial x}\right) + \frac{\partial}{\partial y}\left(\kappa\frac{\partial T}{\partial y}\right) + \frac{\partial}{\partial z}\left(\kappa\frac{\partial T}{\partial z}\right), \tag{3}$$

where T is the temperature, C_v the heat capacity at constant volume, and κ is the heat conductivity coefficient. The effect of thermal conductivity is very important for the modeling of laser plasma phenomena (see Section 4). The solution of this equation is obtained by means of the local one dimensional approximation method. We solved it using an implicit scheme and the marching method.

3   Modeling of the Richtmyer-Meshkov Instability. Comparison with the Shock Tube Experiment

By using the NUT code, we have performed a series of simulations modeling shock tube experiments made at G. M. Krzhizhanovsky Power Institute Moscow [5]. We
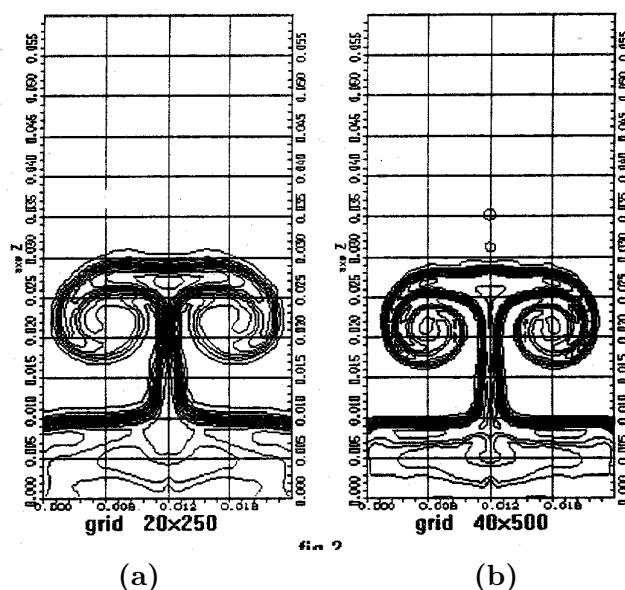
Figure 1: Density peaks near the Ar-Xe contact boundary after the transmission of the shock wave, (a) the grid 20×250, (b) the grid 40×500 (the first figure denotes the number of knots in the transverse direction, the second one in the longitudinal direction).

have modeled the development of a perturbation of the contact boundary between two gases (argon and xenon) when the shock wave with the velocity corresponding to Mach number of 3.5 is passing through (i.e. the shock wave velocity is equal to 3.5 of the sound velocity in the given medium). The first calculation was done in a 2D geometry, with initial sinusoidal perturbation of wavelength $\lambda = 24$mm, and amplitude $a_0 = 5$mm (the distance from the bottom to the top of a spike is 10 mm). The initial pressure was equal to 0.5 atm. The calculations of the contact boundary perturbation were performed by making use of different grids. It was shown that as soon as the number of grid nodes in the form of the "mushroom-like perturbations" increases there appear so called "additional details", so one is able to simulate small-scale perturbations. The temporal dependence of the amplitude growth is practically the same for the 20×250 and 40×500 grids. Figure 1 illustrates the shape of perturbation contact boundary at $t = 170$ mks obtained with the 20×250 and 40×500 grids.

In the next test, we compared our results with the results of the other group from the Moscow Institute of Physics and Technology [6]. Figure 2a illustrated the growth of perturbations of the contact boundary between Helium and Xenon gases. The initial pressure was 0.5 barr, Mach number 2.5, and initial disturbance wavelength 8 mm. We have obtained good agreement in the speed of the perturbation growth. Figure 2b
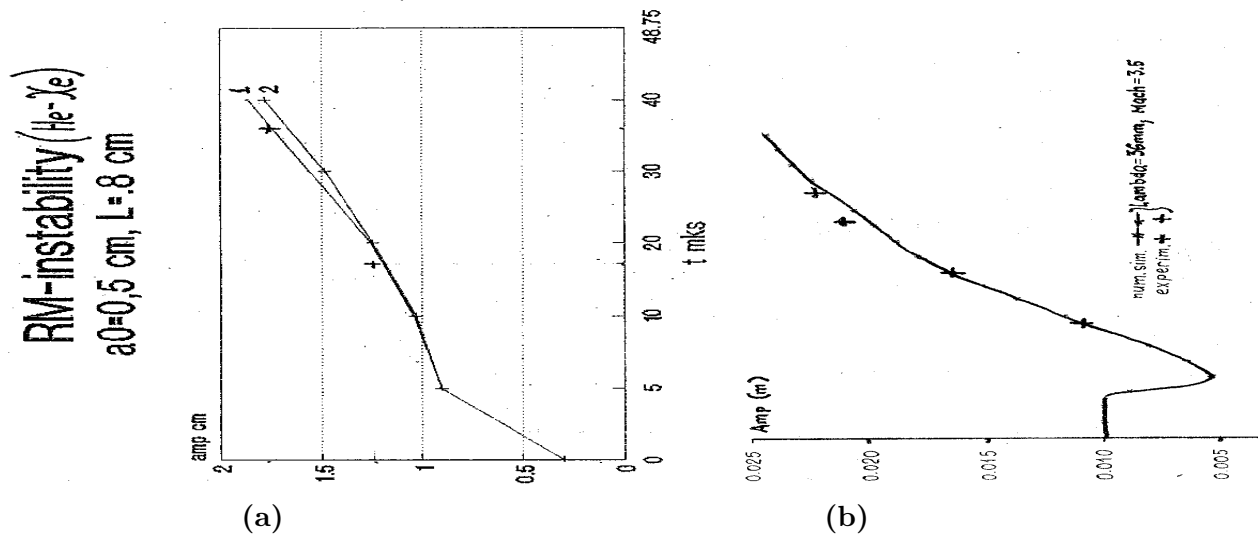
Figure 2: (a) The comparison of perturbation speed growth. Series 1–NUT, Series 2–MPTI, $p_0 = 0.5$ barr, $M_x = 2.5$. (b) The contact boundary perturbation amplitude growth versus the time for the wavelength $\lambda = 36$ mm and $\lambda = 18$ mm. The "cross" denotes the perturbation amplitude obtained in the shock tube experiments for the case $\lambda = 36$ mm.

shows the calculated growth of the amplitude (here and hereafter an "amplitude" means the distance from the "bottom" to the "top of the spike" of the contact boundary) for different perturbation wavelengths. The calculations showed good agreement between the amplitude growth velocity and the experimental data.

The experimental data were obtained at the G. M. Krzhizhanovsky Power Institute. Moreover, it is possible to reproduce the form of the perturbation at the nonlinear stage of the instability development (a so-called "mushroom"-like structure) [5]. Figure 3 illustrates the form of the contact boundary at time $t = 100$ mks obtained by experiment (a) and in the calculation (b).

A series of 3D experiments have been carried out. The initial perturbation of the contact boundary (argon-xenon) had the form:

$$Z_c^{pert} = Z_c^0 + a_0 \cos(k_x x) \cos(k_y y)$$

where $a_0 = 5$ mm, $k_x = 2\pi/\lambda_x$, $k_y = 2\pi/\lambda_y$, $\lambda_x = \lambda_y = 36$ mm. An incident shock wave was propagating along the axis Z, and its velocity corresponded to the Mach number of 3.5. As follows from [1], at a linear stage the perturbations in 2D and 3D geometry have the same velocity provided the following condition is fulfilled:

$$k_{2D} = 2\pi/\lambda_{2D} = k_{3D} = \sqrt{(2\pi/\lambda_x)^2 + (2\pi/\lambda_y)^2}$$

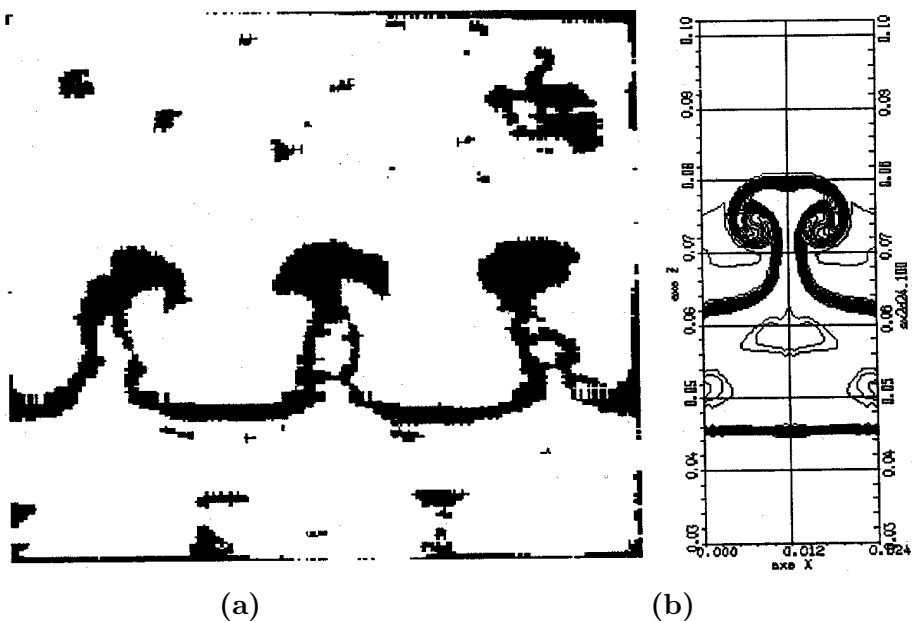**(a)**   **(b)**

Figure 3: (a) The experimental data borrowed from [5]. (b) The isodensity lines obtained in the calculation at the same moment, $t = 100$ ms for $\lambda = 24$ mm.

wherefrom $\lambda_{3D} = \sqrt{2}\lambda_{2D}$, if $\lambda_x = \lambda_y = \lambda_{2D}$.

From this follows that in 3D geometry, the perturbations with $\lambda_{3D} = 36$ mm should be compared to the 2D perturbations with $\lambda_{2D} \approx 24$ mm. Figure 4 shows the growth of the perturbation amplitudes for both 3D and 2D geometries. It is seen that at the nonlinear state ($ka > 3$, where k is the wave number and a the current amplitude) the perturbations in 2D grow more slowly. This may be explained by the fact that, due to the growth of Kelvin-Helmholtz instability near the top of the spike, the processes of the vortex structure formation and the "blurring" of such a spike are faster (see e.g. [7]). In order to investigate the influence of the period on the development and formation of the vortex structures, we have performed a calculation of the Ar-Xe contact boundary perturbation development in the case where

1. initial perturbation is the sinusoid with wavelength $\lambda = 24$ mm;

2. the calculated region of the X axis is twice as high and the initial perturbation has the form:

$$Z_c(x,y) = \begin{cases} Z_0 + a_0 \cos(k_x x), & \text{if } 0 \leq x \leq \lambda_x/2; \\ 0, & \text{if } \lambda_x/2 \leq x \leq \lambda_x, \end{cases}$$
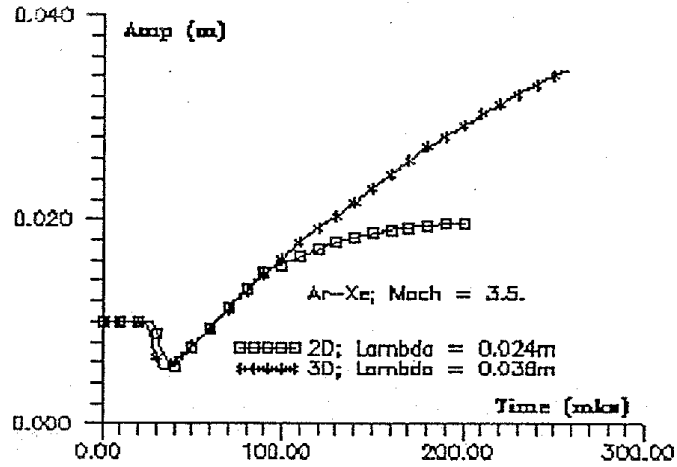
Figure 4: The contact boundary perturbation amplitude growth versus time for 3D perturbation (λ = 36 mm) and 2D perturbation (λ = 24 mm).

that is, "an absolutely elastic wall" (i.e. $u = -u$) is placed at $x = \lambda = 24$ mm;

3. the case of "free flow through a wall" ($du/dx = 0$, at $x = \lambda/2$). The dependence of the perturbation amplitude growth is close to that which is observed when the "wall" is located at the point $x = \lambda/2$, but there are some differences.

The shape of the perturbation (second case) at time $t = 170$ mks, is shown in Fig. 5a, while Fig. 5b illustrates the amplitude development of the contact boundary corresponding to all three cases. One can see that "solitary perturbation" has a bigger amplitude at $t = 200$ mks.

Together with professor S. G. Zaitsev's group from Krzhizhanovsky Power Institute, we have studied the problem of two wave perturbation interaction at the RMI. Now we are demonstrating the first results of such simulations. We calculated until two variants for the case of He-Xe interface, initial pressure 0.5 barr, Mach number 2.5 (Figure 6a,b): 1) $\lambda_1 = 18$ mm, $a_1^0 = 10$ mm, and $\lambda_2 = 9$ mm, $a_2^0 = 5$ mm with the distance between the tops $0.5(\lambda_1 + \lambda_2)$; 2) $\lambda_1 = 18$ mm, $a_1^0 = 10$ mm, and $\lambda_2 = 9$ mm, $a_2^0 = 5$ mm, but the distance between the tops is $1.5\lambda_1 + 0.5\lambda_2$.

One can see the development of perturbations in variant 1 and variant 2. The speed of perturbation growth in variant 1 is bigger than in variant 2 (Figure 6c).
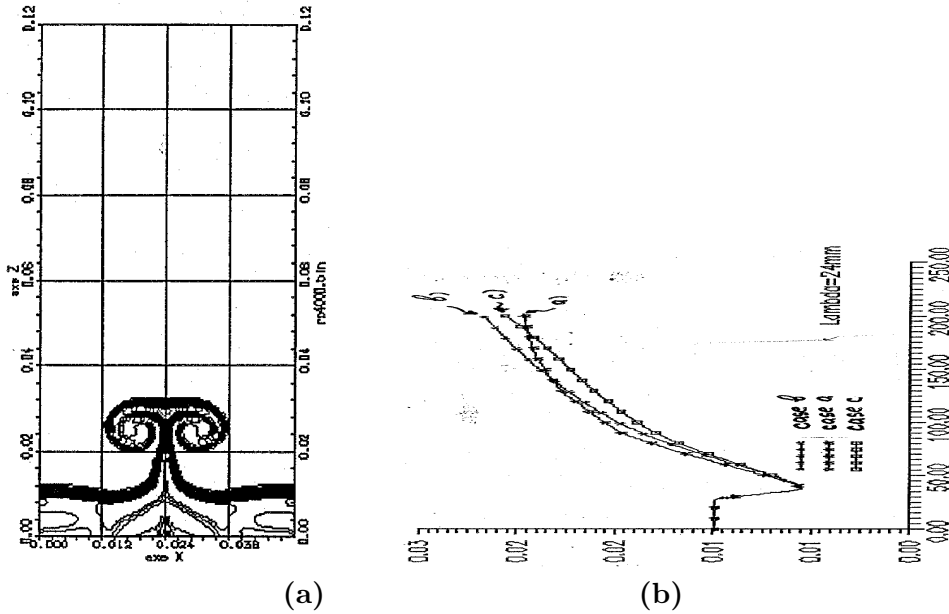
(a)   (b)

Figure 5: (a) The density isolines near the Ar-Xe contact boundary for the case of a "solitary perturbation (case 2) $\lambda = 24$ mm, $a_0 = 5$ mm. (b) The contact boundary perturbation amplitude growth for the cases 1. an elastic wall at $x = 12$ mm, 2. "distant elastic wall" at $x = 24$ mm, 3. the boundary conditions of the "free flow through a wall".

4   Richtmyer-Meshkov Instability in a Laser Target

In contrast to the shock-wave experiments, the development of instabilities in laser targets is essentially influenced by the electron heat conductivity. The heat conductivity process is described by equation (3). A one-temperature approximation that is true in the dense compressed target (where the electron-ion exchange time is small due to high plasma density) is considered.

In order to calculate the development of perturbations in the target we used, as the initial data, the 2D Lagrangian code "Atlant" [8]. Note that most of the Lagrangian codes used in the target compression calculations would not allow us to obtain a "mushroom-like" structure at the contact boundary, due to a strong deformation of the calculation cells. Figure 7a illustrates a dependence of the "shell-fuel" contact boundary velocity on the time of the shell, and Figure 7b demonstrates a distribution of the plasma density on the radius by the moment of the retardation.

In order to calculate this problem using the NUT code, we have set three subregions.
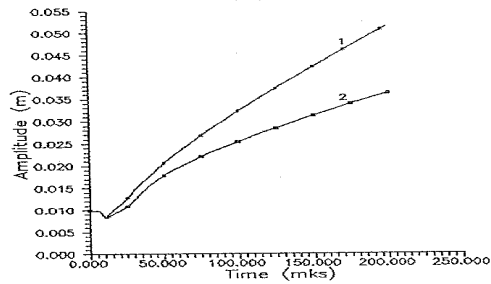
1. The first subregion with the DT fuel of density $\rho_F = 0.05 \text{g/cm}^3$.
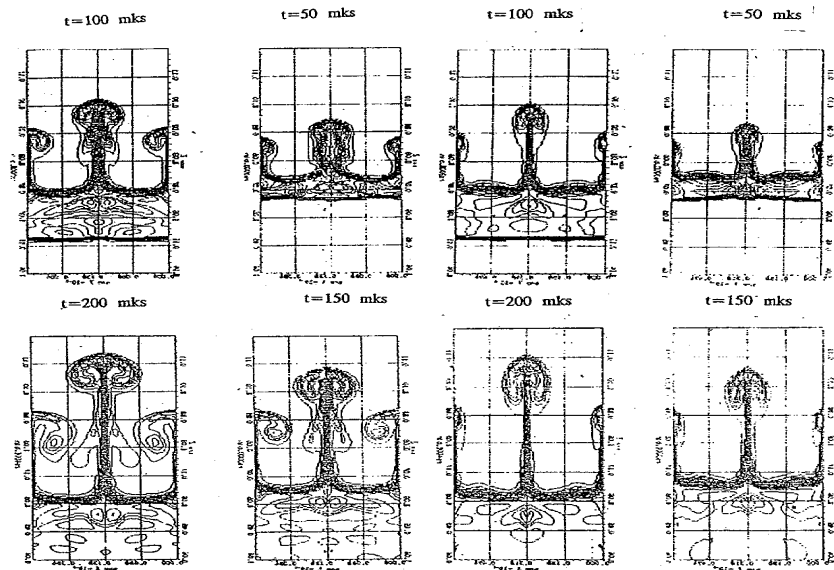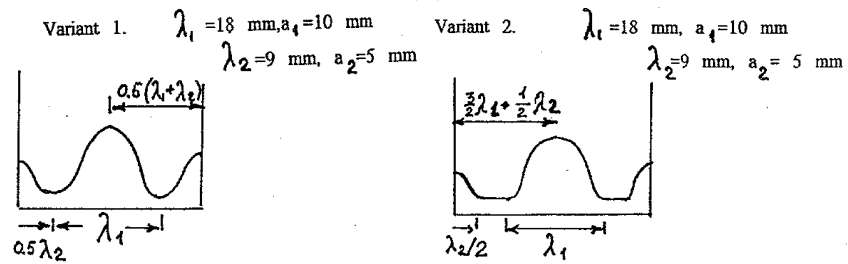
Figure 6: (a), (b) The development of the two wave perturbation for variant 1 and variant 2 (He-Xe, $M = 2.5$). (c) The contact boundary perturbation amplitude growth for variant 1 and variant 2.
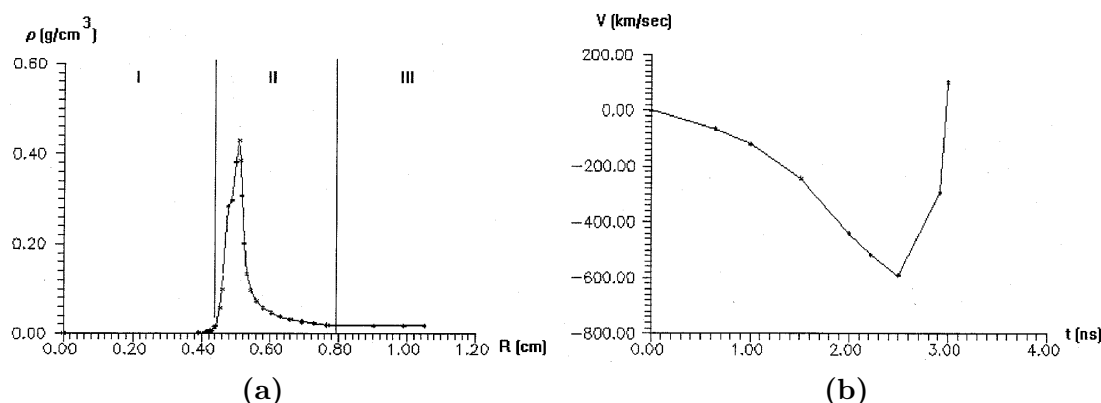
Figure 7: (a) The dependence of the shell-fuel contact boundary velocity on the time obtained by the "Atlant" code. (b) The distribution of the shell plasma density versus the radius at the beginning of retardation.

2. The second subregion with the unevaporated part of a shell. The averaged density and the region thickness were varied in the calculations so as to obtain $\rho_S L = 10 \mathrm{g/cm}^3$.

3. The third region is the corona. In the calculations, the values of the average corona density were $\rho_C = 3 \mathrm{mg/cm}^3$ and $\rho_C = 150 \mathrm{mg/cm}^3$.

   The initial temperature in the corona was equal, respectively, to 1 keV and 0.02 keV. The temperature in the subregions I and II was calculated so as to make the pressure at $t = 0$ constant within the whole region. The shock wave moved from the DT fuel to the shell with a relative velocity of 250 km/s (in one of the variants, 500 km/s).

5   The analysis of the calculation results

We performed 2D calculations of the "shell-fuel" contact boundary perturbation for different wavelength of $\lambda = 5$ mkm, 10 mkm, 20 mkm, and the initial amplitude $a_0 = 2$ mkm. The behavior of the instability is strongly affected by the heat conductivity. First, the heat flow from the corona to the shell leads to the formation of a shock wave moving from the corona to the DT fuel towards the first shock wave, which moves from the DT to the shell. As a result, we obtain the density and temperature profiles which are different from those which had emerged in the calculations without heat conductivity (Figure 8). Second, the heat conductivity leads to a "blow-up" of the vortex structure near the top of the spike, so that in variant I (where $\rho_S = 0.1 \mathrm{g/cm}^3$, $\rho_C = 3 \mathrm{mg/cm}^3$, and the shock wave velocity is $w = 500 \mathrm{km/s}$), the "mushroom-like structure" was
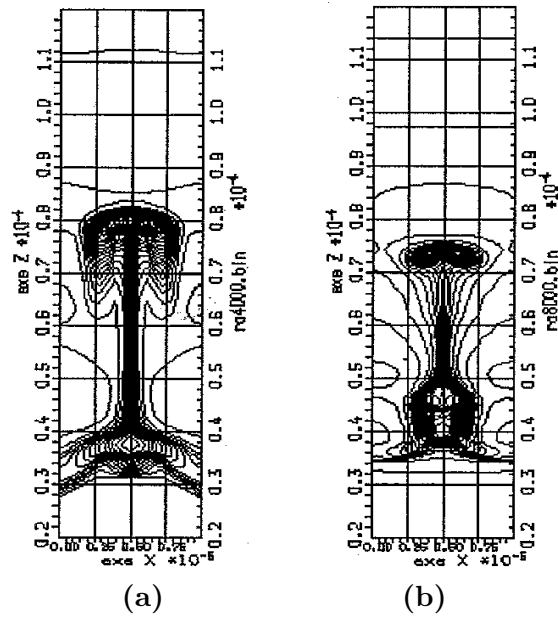
Figure 8: (a) The plasma density isolines near the "shell-fuel" and the "shell-corona" contact boundaries at $t = 0.4$ ns, (from the moment of the shock wave transmission through the first contact boundary) in the case without heat conductivity. (b) The plasma density isolines near the contact boundaries at $t = 0.4$ ns in the case with heat conductivity.

never formed, while in the case without heat conductivity it was clearly observed. We performed calculations with $w = 250$km/s, but with a higher density of the shell (variant 2: $\rho_S = 0.2$g/cm^3, variant 3: $\rho_S = 0.8$g/cm^3, variant 4: $\rho_S = 0.8$g/cm^3, $\rho_C = 150$mg/cm^3).

In variant 4, the corona density was increased, and the temperature, correspondingly, was decreased. As a result, the heat flow from the corona toward the shell had been suppressed. The above calculations were made on a grid of 10×400.

Variant 3 was repeated on a grid of 20×800. The results obtained were close to those derived on a 10×400 grid, that is, the hydrodynamic processes with the conductivity can be simulated with satisfactory accuracy on the given grids. Figure 8 illustrates the isolines of the shell density at $t = 0.063$ ns and $t = 0.237$ ns without heat conductivity. Figure 8b shows the density isolines in the shell. The calculation was done with the allowance of the heat conductivity effect.

6   Conclusion

1. The NUT code allows one to numerically model the development of such complicated phenomena as the Richtmyer-Meshkov instability up to its nonlinear stage, when there occurs the vortex structures, the destruction of fluxes, and the formation of turbulent mixing zones. The comparison of numerical calculations with the results from the shock tube experiments has demonstrated good agreement of the amplitude growth velocity and the shape of the contact boundary perturbation.

2. The development of instability at the "shell-fuel" contact boundary has some peculiar features in the high-temperature plasma of the laser targets. They are due to the influence of a nonlinear heat conductivity. The heat flow at high temperature of the fuel, can reduce the velocity of the perturbation development.

References

[1] Richtmyer, R. D. (1989) Comm. Pure and Appl. Math, 13, n.2, p.297.

[2] Meshkov, E. E., (1969), Isv. Akad. Nauk SSSR, Mekhanika Zhidkosti i Gaza, N5, p.151.

[3] Taylor, G., (1950) Proc. Roy. Soc., 201A, p.191.

[4] Vjaznikov, K. V., Tishkin, V. F., Favorsky, A. P., (1989) Matematicheskoe modelirovanie, v.1, no.5, p.95.

[5] Aleshin, A. N., Lazareva, E. V., Zaytsev, S. G., Rozanov, V. B., Gamaly, E. G., Lebo, I. G., (1990) Dokladi Akademii Nauk SSSR, Fizika, v.310, no.5.

[6] Belosterkovskii, O. M., Demchenko, V. V., Oparin, A. M., (1994) Doklady Russian Academy of Science, v.39, N2, P.118.

[7] Rozanov, V. B., Zmitrenko, N. V., (1992) Preprint FIAN, no.16.

[8] Lebo, I. G., Popov, I. V., Rozanov, V. B., Tishkin, V. F., Journal of Russian Laser Research, (1994) v.15, no.15, p.136.